Geometric Displacement Analysis of Suramadu Bridge Pylons Using Multi-Temporal UAV LiDAR Point Cloud Data Against the Detailed Engineering Design

Abdurrahman Afiq Yuda Hammaami[a,*], Nain Dhaniarti Raharjo[b], Lalu Muhamad Jaelani[a]
[a]Department of Geomatics Engineering, Institut Teknologi Sepuluh Nopember, Surabaya, 60111, Indonesia
[b]Departemen of Civil Engineering, Politeknik Negeri Malang, Malang 65141, Indonesia

*****Corresponding author: 5016221103@student.its.ac.id

Abstract. The Suramadu Bridge is a vital infrastructure connecting Java and Madura Islands. Pylons, as key components of cable-stayed bridges, are susceptible to geometric changes due to sea wave exposure, wind loads, and increasing traffic volume. This study analyzes the geometric displacement of pylons by comparing two periods of UAV LiDAR point cloud data acquired on 5 January 2026 and 2 February 2026 against the Detailed Engineering Design (DED). Data acquisition was conducted using a DJI Matrice 350 UAV with a Geosun GS-260H LiDAR sensor. The geometric analysis encompasses six dimensional parameters and pylon tilt calculated from the combined centroid of both pylon legs. Accuracy validation using ICP points based on SNI 9135-2:2023 confirmed both periods achieved Class 2 accuracy at 1:2,500 scale. The upper width parameter (L1) recorded the largest deviation of 186 mm on the Madura pylon in Period 3, while the middle thickness (T2) was identified as the most critical parameter due to consistently negative deviation, reaching 134 mm on the Madura pylon in Period 5. The Mean Absolute Error indicated that the MDR pylon (51 mm) exhibited greater dimensional change intensity than the SBY pylon (36 mm). Tilt analysis showed both pylons inclined convergently toward the main span, attributed to cable tension.

Keywords: geometric displacement; LiDAR; mean absolute error; point cloud; pylon; tilt analysis.

I. INTRODUCTION

The Suramadu Bridge is a vital infrastructure connecting Java and Madura Islands, with a total length of approximately 5,438 meters and a width of 30 meters. As one of the largest cable-stayed bridges in Indonesia, the Suramadu Bridge plays a strategic role in accelerating inter-island mobility of people and goods, as well as serving as a pillar of regional development in East Java [1]. As traffic volume increases and the bridge ages, Structural Health Monitoring System (SHMS) becomes essential to maintain the function and safety of the bridge [2].

The Suramadu Bridge stands over the sea crossing the Madura Strait, exposing its piers and foundations to an aggressive environment. Corrosion caused by high humidity and seawater waves poses a threat to structural materials [3]. Additionally, strong winds have the potential to affect structural resistance when passing through the bridge structure [4]. Temperature factors can also cause structural deformation in pylons (main supporting towers) and material fatigue [5]. Increasing vehicle volume has been proven to amplify vibration and stress responses on cables and girders [6]. All of these factors can cumulatively affect the geometric integrity of pylons over the long term.

In cable-stayed bridges, the pylon is a key component that receives and distributes forces transmitted from cables and girders [7]. Small displacements occurring in pylons can affect force equilibrium and the overall structural health of the bridge [8]. Minor damage to the Suramadu Bridge structure must be addressed promptly, as if neglected, structural elements may weaken and threaten the projected 100-year bridge lifespan [9].

Monitoring geometric displacement of bridge structures using Light Detection and Ranging (LiDAR) has been widely implemented in recent years [10]. LiDAR is capable of acquiring structural geometry with precise three-dimensional coordinates within minutes, including hard-to-reach structures [11]. The resulting point cloud provides a highly detailed representation of bridge structures, enabling early detection of potential structural problems [12]. Multi-temporal LiDAR data allows more accurate deformation analysis through inter-epoch registration and spatial displacement comparison on structural surfaces [10].

This study was conducted to determine the magnitude of geometric displacement of pylons based on multi-temporal LiDAR point cloud data comparison, and the magnitude of geometric displacement of pylons against the Detailed Engineering Design (DED). The limitations applied include the use of only 2 out of 8 available point cloud datasets, the analysis focuses solely on displacement values without modeling the bridge deck or external factors such as wind, temperature, and traffic loads, and the DED was used as the sole reference without comparing results against structural or bridge standards.

This study aims to identify and quantify the geometric displacement of pylons through multi-temporal LiDAR point cloud data comparison, and to identify the magnitude of geometric displacement of the Suramadu Bridge pylons against the DED. The results are expected to provide precise geometric information and support the development of LiDAR-based structural monitoring methods as part of the long-term monitoring system for the Suramadu Bridge.

Through comprehensive analysis of Mean Absolute Error (MAE) values, inter-period dimensional changes, and tilt measurements, the study identifies which pylon requires prioritized attention in structural monitoring and maintenance programs. The results are expected to provide precise geometric information and support the development of LiDAR-based structural monitoring methods as part of the long-term monitoring system for the Suramadu Bridge.

II. METHODOLOGY

2.1 Study Area

The study was conducted on the pylons of the Suramadu Bridge located in the Madura Strait, connecting Surabaya City and Bangkalan Regency. The bridge consists of three sections: the Surabaya causeway, the main bridge, and the Madura causeway. The cable-stayed section features two main pylons as the research objects, namely the Surabaya-side pylon (SBY) and the Madura-side pylon (MDR).

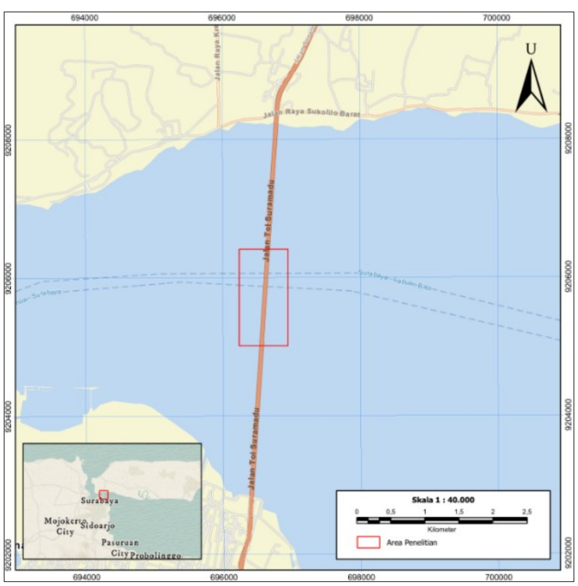

Figure 1 Research Area, Located on the Main Span of the Suramadu Bridge

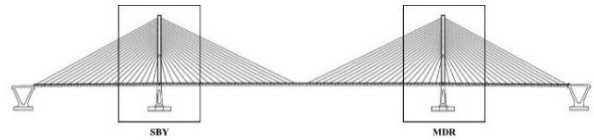

Figure 2 Main Bridge of the Suramadu Bridge

Fig. 2 presents the design of the Suramadu Bridge main bridge, which consists of pylons, cables, and the bridge deck. The focus of this study is on the pylons (indicated by the black box), the bridge components that receive loads from the bridge deck.

2.2 Tools and Materials

Data acquisition was conducted using a DJI Matrice 350 UAV equipped with a Geosun GS-260H LiDAR sensor. Control Point (CP) and Independent Check Point (ICP) measurements were performed using HI-Target GNSS equipment for registration and accuracy validation. LiDAR data processing was carried out using gAirhawk and CloudCompare software, while 3D model analysis was performed using Autodesk Civil 3D software.

The data used in this study include: (1) two sets of LiDAR point clouds acquired in Period 3 on 5 January 2026 and Period 5 on 2 February 2026, (2) the Detailed Engineering Design (DED) data of the Suramadu Bridge as a geometric reference, and (3) control point measurement data consisting of Easting (E), Northing (N), and Elevation (H) coordinates.

Period 3 data were acquired under hot and sunny weather conditions, representing the typical thermal state experienced by the bridge structure under high solar radiation exposure. In contrast, Period 5 data were collected during overcast conditions with lower ambient temperatures, providing a comparative scenario under reduced thermal loading. This selection of two periods from the available eight datasets allows for an initial assessment of dimensional variations under different thermal conditions, though additional acquisition periods would be necessary to establish definitive long-term deformation trends.

2.3 Data Acquisition

Data acquisition was carried out from December 2025 to April 2026 with the measurement stages as illustrated in Fig. 3. The first stage was the measurement of a Benchmark (BM) point located at the Kenjeran Police Station yard using GNSS with the static method to obtain reference coordinates. Subsequently, point cloud data acquisition was performed using a DJI Matrice 350 RTK UAV equipped with a Geosun GS-260H LiDAR sensor with the Post-Processing Kinematic (PPK) method. The final stage was the measurement of CP and ICP points acquired using GNSS. The CP and ICP points utilized visible objects on the bridge pylons to facilitate the registration and validation stages.

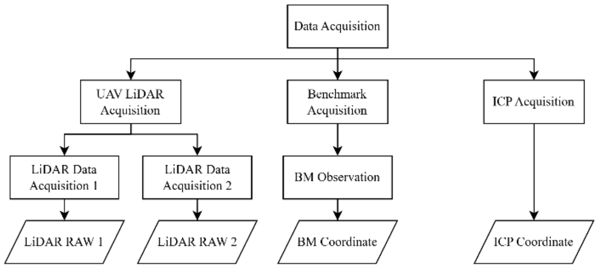

Figure 3 Data Acquisition Steps

2.4 Data Processing

The data processing in this study followed a series of sequential stages as presented in Fig. 4. The first stage involved processing the raw LiDAR data with PPK correction on the UAV flight trajectory data using base station data to produce accurate point cloud coordinates. The registration stage was performed by selecting corresponding point pairs between the point cloud data and the CP points.

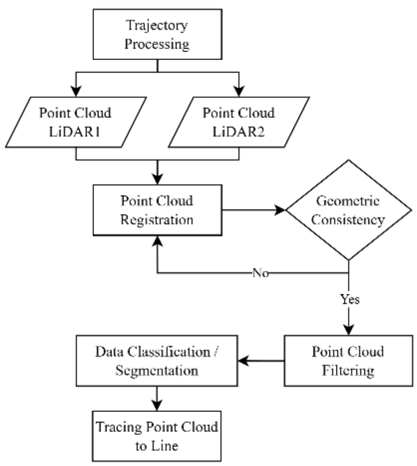

Figure 4 Data Processing Steps

The registration process was performed using the Align feature in CloudCompare software by utilizing the CP points measured in the field as tie points. After both sets of point cloud data were registered, accuracy validation was calculated using four ICP points. Geometric validation of the data was conducted by computing the horizontal and vertical RMSE values from the LiDAR data using the following equations:

$$RMSE_h = \sqrt{\frac{\sum_{i=1}^{n}[(\Delta X_i)^2 + (\Delta Y_i)^2]}{n}} \quad (1)$$

$$RMSE_z = \sqrt{\frac{\sum_{i=1}^{n}(\Delta Z_i)^2}{n}} \quad (2)$$

where ΔXi is the difference between XLiDAR and Xref, and ΔYi is the difference between YLiDAR and Yref. ΔZi is the difference between ZLiDAR and Zref, while n is the number of check points. From the obtained RMSEh and RMSEz values, the Circular Error 90% (CE90) and Linear Error 90% (LE90) were calculated using Eq. (3) and Eq. (4). The results were then classified based on SNI 9135-2:2023 regarding the geometric accuracy of point cloud-based geospatial data.

$$CE90 = 1.5175 \times RMSE_h \quad (3)$$

$$LE90 = 1.6499 \times RMSE_z \quad (4)$$

The next stage involved manual segmentation and filtering in CloudCompare software to separate the pylon point cloud from other bridge elements such as the deck, cables, and noise from objects surrounding the pylon. This process was performed manually to ensure accurate separation of the pylon structure. The subsequent stage was constructing a geometric model by tracing lines on the point cloud surface to obtain a 3D wireframe model as shown in Fig. 5

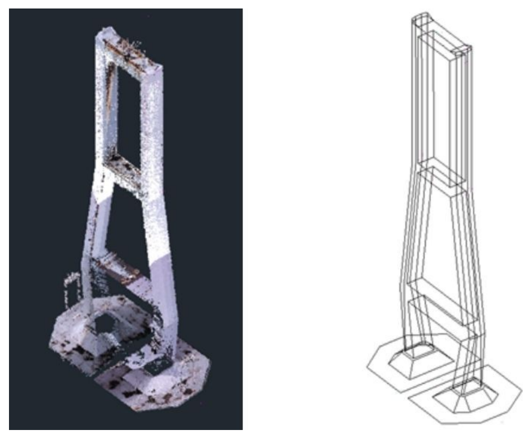

Figure 5 Pylon Point Cloud and 3D Wireframe Results

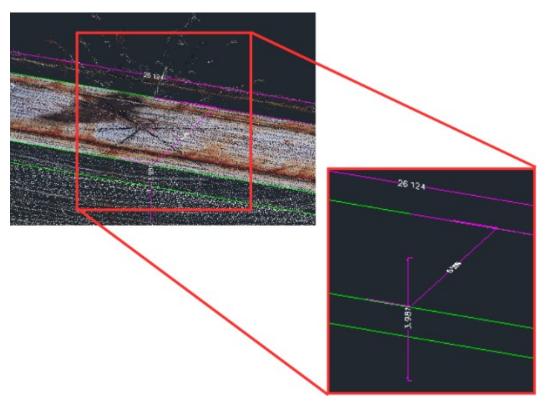

Figure 6 measurements on a 3D model

From this 3D model, measurements were performed on the parameters used for comparison, and the centroid (center point) of the pylon was determined to calculate the tilt value of the observed pylon. The measurement results were then compared against the available DED using Eq. (5).

$$\Delta d = d_{LiDAR} - d_{DED} \tag{5}$$

Where Δd is the dimensional difference (m), dLiDAR is the parameter value measured from the point cloud data, and dDED is the parameter value from the DED. From the resulting differences, the Mean Absolute Error (MAE) was calculated using Eq. (6) as the average value of the comparisons obtained.

$$MAE = \frac{1}{n}\sum_{i=1}^{n}|\Delta d_i| \tag{6}$$

Where MAE is the mean absolute deviation (m), Δdi is the absolute value of the difference for the i-th parameter, and n is the number of measured parameters.

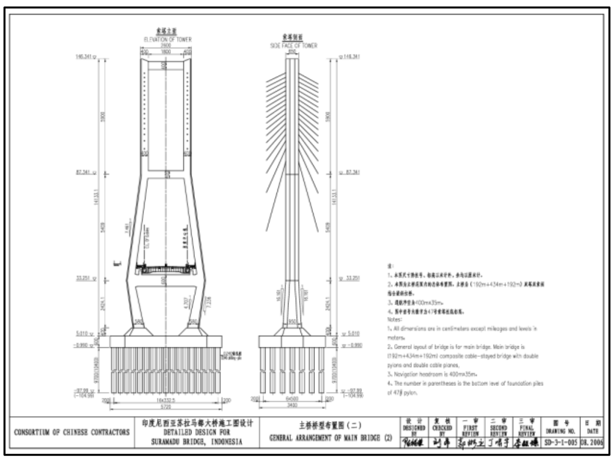

Figure 7 DED of the Suramadu Bridge Pylon [13]

MAE was used because the analyzed parameters have both positive and negative differences, thus absolute values are required to prevent opposing deviations from canceling each other out. MAE was used to perform an overall comparison by averaging all pylon dimensional parameters against the DED.

In addition to determining the dimensional differences between measurement results and the DED, the tilt value of the pylon was determined based on the centroid displacement between the base and top sections of the structure using Eq. (7).

$$\theta = \arctan\left(\frac{\sqrt{(\Delta X)^2 + (\Delta Y)^2}}{\Delta Z}\right) \tag{7}$$

Where θ is the tilt value of the pylon relative to the vertical line (°), ΔX and ΔY are the horizontal coordinate differences between the upper and lower centroids (m), and ΔZ is the elevation difference between the upper and lower centroids (m). The centroid values were determined from the average coordinates of the pylon cross-section points at each respective elevation.

2.5 Lidar Point Cloud Quality

The accuracy validation of LiDAR data was performed using four ICP points measured with GNSS. The calculation of RMSEh, RMSEz, as well as CE90 and LE90 values was conducted based on SNI 9135-2:2023 as presented in Tab. 1.E

Table 1
Calculation of CE90 and LE90 for Period 3 and Period 5 Data

Parameter	Periode 3 (m)	Periode 5 (m)
$RMSE_h$	0.161	0.073
$RMSE_z$	0.198	0.194
CE90	0.244	0.110
LE90	0.328	0.319

Based on Tab. 1, Period 5 demonstrated better accuracy compared to Period 3 across all parameters, with smaller CE90 and LE90 values. According to SNI 9135-2:2023, at a 1:2,500 scale, both periods achieved Class 2, where CE90 and LE90 values were below the tolerance limits of 75 cm and 37.5 cm respectively. At a 1:5,000 scale, both periods achieved Class 1. Accordingly, the point cloud data from both periods were deemed suitable for displacement analysis as they possessed equivalent quality.

2.6 Geometric Analysis Parameters

The geometric analysis was performed on six dimensional parameters for each pylon as presented in Tab. 2. In addition to dimensional parameters, pylon tilt analysis was also conducted by calculating the combined centroid position of both pylon legs at the base and top elevations, then determining the angular deviation of the structural axis from the ideal vertical line using Eq. (7).

Table 2
Geometric Analysis Parameters

Parameter	Code	DED (m)
Upper Width	L1	26
Center Width	L2	26
Upper Thickness	T1	4
Center Thickness	T2	4
Upper Side Thickness	T3	6.5
Lower Side Thickness	T4	6.5

Deviation classification was established based on three categories: (1) |Δd| ≤ 30 mm, categorized as not considered a displacement; (2) 30 mm < |Δd| ≤ 100 mm, categorized as requiring attention; and (3) |Δd| > 100 mm, categorized as a significant change. This classification serves as one of the assessment indicators used to classify the conditions occurring on the bridge in accordance with the obtained measurements.This value is a criterion proposed by the author based on the geometric accuracy of the LiDAR data and the sensor specifications.

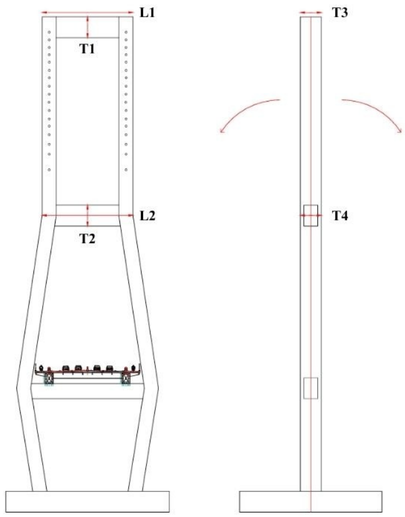

Figure 8 Geometric Parameters in 3D Models

III. RESULT AND DISCUSSION

3.1 Geometric Measurement Results

Geometric parameter measurements were performed on the three-dimensional model reconstructed from point cloud data using Civil 3D software as shown in Fig. 6. Tab. 3 presents the dimensional measurement results from Period 3 data, and Tab. 4 presents the data measured in Period 5. The measurements encompass the predetermined parameters, as well as the determination of centroid points as shown in Fig. 7 which were used for tilt calculation.

Table 3
Geometric Measurements - Period 3

Code	Pylon SBY (m)	Pylon MDR (m)
L1	26.124	26.186
L2	25.982	26.025
T1	3.981	4.020
T2	3.914	3.962
T3	6.515	6.499
T4	6.500	6.500

Table 4
Geometric Measurements - Period 5

Code	Pylon SBY (m)	Pylon MDR (m)
L1	26.013	25.996
L2	26.020	26.009
T1	3.983	4.016
T2	3.966	3.866
T3	6.500	6.500
T4	6.500	6.500

At a glance, the pylon dimensional values in both periods produced measurements that were relatively consistent with the DED dimensions. Therefore, to obtain the magnitude of deviation for each parameter against the design specifications, difference calculations were performed to determine the deviation from the available data.

3.2 Deviation Analysis Against DED

To obtain the deviation of measurement results against design dimensions, the differences between measured values in each period and DED values were calculated.

Based on Tab. 5, the majority of parameters showed deviations of less than 30 mm. Parameters L2, T1, T3, and T4 across both pylons and both periods had difference values not exceeding 25 mm, thus these differences were not categorized as geometric displacement.

Parameter L1 in Period 3 showed significant positive differences, namely +124 mm for the SBY pylon and +186 mm for the MDR pylon, exceeding the 100 mm threshold which indicates that the measured upper width was larger than the DED. In Period 5, the L1 difference decreased drastically to +13 mm (SBY) and −4 mm (MDR), which in contrast showed excellent conformity with the DED.

Table 5
Measurement differences compared to DED, as well as the resulting MAE values

Code	P3 SBY (mm)	P3 MDR (mm)	P5 SBY (mm)	P5 MDR (mm)
L1	+124	+186	+13	−4
L2	−18	+25	+20	+9
T1	−19	+20	−17	+16
T2	−86	−38	−34	−134
T3	+15	−1	0	0
T4	0	0	0	0
MAE	44	45	14	27

Parameter T2 emerged as the most critical parameter because all of its difference values were negative, indicating that the middle thickness of the pylon was consistently smaller than the DED across both pylons and both periods. In Period 3, T2 differences were recorded at −86 mm for the SBY pylon and −38 mm for the MDR pylon. The condition became more critical in Period 5, particularly for the MDR pylon which recorded a difference of −134 mm, making it the largest deviation among all parameters.

Differences in point cloud quality between periods, influenced by varying atmospheric conditions during acquisition, may affect laser pulse penetration and surface definition accuracy. Manual segmentation of pylon point clouds from surrounding bridge elements (deck, cables, noise) introduces operator-dependent variability in boundary definition, while the wireframe digitization process in Civil 3D relies on subjective interpretation of point cloud surfaces to trace structural edges.

3.3 Inter-Period Deviation Analysis

In addition to comparing measurement results against the DED, inter-period difference calculations were also performed to identify dimensional changes occurring within the observation timeframe. The calculation results of P5 − P3 for both pylons are presented in Tab. 6.

Parameter L1 showed the largest inter-period change with a difference of −111 mm for the SBY pylon and −190 mm for the MDR pylon, both exceeding the significance threshold. This change indicates that the upper width dimension of the pylon in Period 5 was smaller compared to Period 3. Parameter T2 on the MDR pylon also showed a significant change of −96 mm, which is consistent with the dimensional decrease trend in that parameter. The pier thickness parameters (T3 and T4) demonstrated the highest stability, with inter-period differences not exceeding 15 mm for both pylons.

Table 6
Calculation of the Difference Between Measurement Periods

Code	Selisih Antar Periode (P5 – P3)	
	SBY (mm)	MDR mm)
L1	-111	-190
L2	+38	-16
T1	+2	-4
T2	+52	-96
T3	+15	+1
T4	0	0
MAE	36	51

3.4 Mean Absolute Error Analysis

The MAE values provide an overview of pylon geometric deviation. In Period 3, the MAE for the SBY pylon was 44 mm and 45 mm for the MDR pylon, indicating relatively equal aggregate deviation between both pylons. In Period 5, the MAE for the SBY pylon decreased to 14 mm, while the MDR pylon recorded 27 mm. The decrease of SBY MAE in Period 5 indicates excellent geometric conformity with the DED, whereas the MDR MAE which remained relatively high was primarily influenced by parameter T2.

The inter-period MAE values of 36 mm for the SBY pylon and 51 mm for the MDR pylon indicate that the MDR pylon experienced greater dimensional change intensity within the observation period.

3.5 Pylon Tilt Analysis

The tilt analysis was performed by calculating the average centroid position of both pylon legs at the base elevation (~9 m) and the top elevation (~145 m). The calculation results are presented in Tab. 7. The calculation results showed that both pylons experienced convergent inclination toward the main span of the bridge. The SBY pylon, located on the southern side, had its top displaced northward (toward the central span), while the MDR pylon, located on the northern side, had its top displaced southward (toward the central span). This inclination pattern was consistent across both observation periods.

Table 7
Pylon Tilt Analysis

Pylon	Periode	θ (°)	ΔH (mm)	Arah	Keterangan
SBY	P3	0.129	306	North	Middle Span
SBY	P5	0.144	342	North	Middle Span
MDR	P3	0.209	494	South	Middle Span
MDR	P5	0.135	321	South	Middle Span

The SBY pylon showed a horizontal displacement of 306 mm (0.129°) in Period 3, increasing to 342 mm (0.144°) in Period 5, with an increment of 36 mm. The MDR pylon showed a horizontal displacement of 494 mm (0.209°) in Period 3, decreasing to 321 mm (0.135°) in Period 5, with a reduction of 173 mm. This can be attributed to the tensile forces of the cables which generate a moment causing the pylon tops to be pulled toward the center of the bridge. As illustrated in Fig. 8, both pylons tend to incline toward the center, with the uppermost section being the part with the greatest inclination relative to the base position, or the zero-height level of each pylon.

Figure 9 Illustration of the Pylon's Tilt Angle

3.6 Priority Pylon (Monitoring)

The evaluation of the geometric condition of both pylons was conducted through three indicators, namely dimensional deviation against the DED, MAE values, and tilt. Based on all indicators, the Madura-side pylon (MDR) was identified as the structure requiring more intensive attention compared to the Surabaya-side pylon (SBY).

Parameter T2 on the MDR pylon showed the largest deviation across all measurement comparisons, reaching −134 mm in Period 5. For this parameter, the deviation increased from −38 mm in Period 3 to −134 mm in Period 5. This significant dimensional decrease trend indicates an ongoing geometric change in the middle cross-section of the MDR pylon, which has the potential to affect the cross-sectional capacity in resisting force distribution from the stay cables.

The MAE values of the MDR pylon were consistently higher than those of the SBY pylon, with the disparity becoming more pronounced in Period 5 at 27 mm compared to 14 mm. The inter-period MAE (P5−P3) also showed a similar pattern, namely 51 mm for the MDR pylon compared to 36 mm for the SBY pylon, indicating greater dimensional change intensity in the MDR pylon.

Third, the MDR pylon in Period 3 recorded the largest tilt across all measurement configurations with a displacement of 494 mm (0.209°). Although this value decreased in Period 5, the high variability between periods for the MDR pylon warrants attention in the context of long-term monitoring.

The consistently larger deviations of the MDR pylon compared to the SBY pylon may be influenced by differences in loading characteristics received by each pylon. Differences in span length, cable configuration, and non-uniform environmental exposure between the Surabaya and Madura sides have the potential to produce different force distributions on both pylons. The results obtained from the two observation periods cannot yet definitively distinguish whether the detected deviations represent permanent deformation due to structural degradation or cyclic variations influenced by loading conditions during data acquisition.

The SBY pylon demonstrated a relatively more stable geometric condition, with all parameters in Period 5 having deviations not exceeding 34 mm against the DED. Although parameter T2 on the SBY pylon also showed consistently negative deviations, the magnitudes remained within the attention-required category and had not yet exhibited a concerning progressive trend. Therefore, within the framework of structural monitoring and maintenance prioritization, the Madura-side pylon requires greater attention allocation.

IV. CONCLUSION

Based on the geometric displacement analysis of the Suramadu Bridge pylons through comparison of two periods of UAV LiDAR point cloud data against the DED, it was concluded that geometric displacement values between Period 3 and Period 5 were found in several parameters. The largest change occurred in parameter L1 with a difference of 111 mm for the SBY pylon and 190 mm for the MDR pylon, as well as parameter T2 on the MDR pylon with a change of 96 mm. The pier thickness parameters (T3 and T4) showed the highest conformity with inter-period differences of ≤15 mm.

Displacement against the DED showed that parameter L1 had the largest deviation, particularly in Period 3 with values of 124 mm and 186 mm. However, this was no longer the case for the same parameter in Period 5, in contrast to parameter T2 across Period 3 and Period 5 with a deviation range of 34 mm to 134 mm. The MAE of the MDR pylon (27 mm) was nearly twice as large as the SBY pylon (14 mm) in Period 5, indicating that overall the geometric condition of the MDR pylon had greater deviation from the design specifications, establishing it as the pylon requiring priority in structural monitoring and maintenance.

Both pylons showed convergent inclination toward the main span of the bridge, with the SBY pylon inclining northward and the MDR pylon inclining southward. The SBY pylon showed a tilt of 0.129° with a maximum displacement of ΔH = 306 mm in Period 3, increasing to 0.144° with a maximum displacement of ΔH = 342 mm in Period 5, with an increment of 36 mm between periods indicating a consistent and slightly increasing tilt trend. Meanwhile, the MDR pylon showed a tilt of 0.209° with a maximum displacement of ΔH = 494 mm in Period 3, decreasing to 0.135° with a maximum displacement of ΔH = 321 mm in Period 5, with a reduction of 173 mm. This convergent pattern is indicated as a response to the stay cable tension that continuously pulls the tops of both pylons toward the main span of the bridge.

The comparison results against the DED showed good consistency across the majority of parameters, where the values obtained between pylons and between periods did not show drastically opposing anomalies. The observed value variations between periods, particularly in parameters L1 and T2, may be influenced by several factors during data acquisition, such as differences in point cloud data quality between periods, traffic conditions affecting load distribution on the structure, and different wind and weather conditions at each data acquisition time. In the future, increasing the number of acquisition periods in subsequent research will strengthen the interpretation of the detected variations, whether they are consistent as displacement trends or fluctuations influenced by external factors during measurement.

ACKNOWLEDGEMENT

The authors would like to express their gratitude to PT Terraflow for their assistance in data collection. This research was funded by the Indonesia Endowment Fund for Education (LPDP) on behalf of the Ministry of Higher Education, Science, and Technology of the Republic of Indonesia, and managed under the EQUITY Program (Contract No. 4299/B3/DT.03.08/2025 & No. 3029/PKS/ITS/2025).

REFERENCES

[1] PUPR, "Keberhasilan Pembangunan Suramadu Menjadi Prestasi Membanggakan," Kementerian Pekerjaan Umum dan Perumahan Rakyat (2009).

[2] M. Schlögl, P. Dorninger, M. Kwapisz, M. Ralbovsky, dan R. Spielhofer, "Remote Sensing Techniques for Bridge Deformation Monitoring at Millimetric Scale," PFG, Vol. 90, No. 4 (2022) 391–411. https://doi.org/10.1007/s41064-022-00210-2

[3] A. Setijorini dan A. Ratnaningsih, "Monitoring of Substructure Building of Suramadu Bridge Causeway

Segment on Surabaya Side Based on Corrosion Level," Vol. 6, No. 1 (2022). https://doi.org/10.1108/IJDRBE-03-2020-0018.1

[4] A. F. Bofanda, "Analisa Karakteristik Aliran Angin di Jembatan Suramadu Sebagai Akses Transportasi," Tugas Akhir, Institut Teknologi Sepuluh Nopember (2018).

[5] G. Zhong et al., "Digital Integration of Temperature Field of Cable-Stayed Bridge Based on Finite Element Model Updating and Health Monitoring," Sustainability, Vol. 15, No. 11 (2023). https://doi.org/10.3390/su15119028

[6] T. Lu, J. Liu, T. Guo, L. Zhang, dan Y. Xia, "Traffic-induced Fatigue Damage Evaluation of Long-Span Suspension Bridge Integrating 27-year Monitoring Data," J. Civil Structural Health Monitoring, Vol. 15, No. 7 (2025) 2299–2319. https://doi.org/10.1007/s13349-025-00936-8

[7] B. Nugroho, S. Jepriani, dan S. Juniardi, "Modifikasi Perencanaan Jembatan Mahakam 4 di Kota Samarinda Menggunakan Model Cable Stayed," Jurnal Inersia, Vol. 14, No. 1 (2023) 43–51. https://doi.org/10.46964/inersia.v14i1.373

[8] C. Machelski, M. Hildebrand, dan J. Rybak, "Measurement of Deformation and Force Changes Recorded During Long-Term Monitoring of a Steel Cable-Stayed Bridge," Sensors, Vol. 25, No. 12 (2025). https://doi.org/10.3390/s25123638

[9] M. Iksan, "Jika Pemeliharaan Tidak Dilakukan dengan Baik, Pakar Konstruksi: Jangan Harap Usia Jembatan Suramadu Bisa Sampai 100 Tahun," (2024).

[10] Y. Zhou et al., "High-Precision Monitoring Method for Bridge Deformation Measurement and Error Analysis Based on Terrestrial Laser Scanning," Remote Sensing, Vol. 16, No. 13 (2024). https://doi.org/10.3390/rs16132263

[11] G. Cha, S. H. Sim, S. Park, dan T. Oh, "Lidar-Based Bridge Displacement Estimation Using 3D Spatial Optimization," Sensors, Vol. 20, No. 24 (2020). https://doi.org/10.3390/s20247117

[12] F. S. Brandao dan T. N. Bittencourt, "Deformation Monitoring of Bridges Using Point Clouds," Life-Cycle Performance of Structures and Infrastructure Systems in Diverse Environments (2025) 409–416. https://doi.org/10.1201/9781003595120-49

[13] Consortium of Chinese Contractors, *Suramadu Bridge, Indonesia — Main Bridge (K2+129.50~K2+947.50): Detailed Design (For Construction)*, Vol. 3 of 4, Fascicule 1 of 4. Beijing, China (2006).